Published OnlineFirst July 21, 2017; DOI: 10.1158/2326-6066.CIR-16-0400

Research Article

Cancer Immunology Research

Constitutive IDO1 Expression in Human Tumors Is Driven by Cyclooxygenase-2 and Mediates Intrinsic Immune Resistance

Marc Hennequart[1,2], Luc Pilotte[1,2], Stefania Cane[1,2], Delia Hoffmann[1,2], Vincent Stroobant[1,2], Etienne De Plaen[1,2], and Benoît J. Van den Eynde[1,2,3]

Abstract

Tumors use various mechanisms to avoid immune destruction. Cyclooxygenase-2 (COX-2) expression may be a driver of immune suppression in melanoma, but the mechanisms involved remain elusive. Here, we show that COX-2 expression drives constitutive expression of indoleamine 2,3-dioxygenase 1 (IDO1) in human tumor cells. IDO1 is an immunosuppressive enzyme that degrades tryptophan. In a series of seven human tumor lines, constitutive IDO1 expression depends on COX-2 and prostaglandin E2 (PGE_2), which, upon autocrine signaling through the EP receptor, activates IDO1 via the PKC and PI3K pathways. COX-2 expression itself depends on the MAPK pathway, which therefore indirectly controls IDO1 expression. Most of these tumors carry PI3K or MAPK oncogenic mutations, which may favor constitutive IDO1 expression. Celecoxib treatment promoted immune rejection of IDO1-expressing human tumor xenografts in immunodeficient mice reconstituted with human allogeneic lymphocytes. This effect was associated with a reduced expression of IDO1 in those ovarian SKOV3 tumors and an increased infiltration of $CD3^+$ and $CD8^+$ cells. Our results highlight the role of COX-2 in constitutive IDO1 expression by human tumors and substantiate the use of COX-2 inhibitors to improve the efficacy of cancer immunotherapy, by reducing constitutive IDO1 expression, which contributes to the lack of T-cell infiltration in "cold" tumors, which fail to respond to immunotherapy. *Cancer Immunol Res; 5(8); 695–709.* ©2017 AACR.

Introduction

Clinical results from cancer therapy based on the stimulation of antitumor immune responses has introduced a paradigm shift in oncology. By releasing brakes that repress T lymphocytes, antibodies able to block inhibitory receptors CTLA-4 or PD1 expressed at the surface of T cells can unleash antitumor immunity, inducing durable tumor responses and improving survival of advanced cancer patients (1). However, this favorable outcome is observed in only 20% to 40% of patients. In other patients, tumors appear to establish an immunosuppressive microenvironment that prevents the action of antitumor T lymphocytes. Further progress therefore depends on our ability to understand and target these immunosuppressive mechanisms, which are likely manifold and involve a variety of cellular and molecular pathways.

Tryptophan catabolism has emerged as a factor orchestrating immunosuppression in the tumor microenvironment. Aberrant tumoral expression of cytosolic tryptophan-degrading enzyme indoleamine 2,3-dioxygenase 1 (IDO1) in tumors results in rapid conversion of tryptophan into kynurenine. The resulting microenvironment, depleted in tryptophan and enriched in kynurenine, is immunosuppressive (2, 3). Indeed, tryptophan shortage induces an arrest of T-lymphocyte proliferation, apparently linked to the induction of a GCN2-mediated integrated stress response, whereas kynurenine and other tryptophan catabolites can induce T-cell apoptosis and/or favor the induction of regulatory T cells (4–6). In humans, IDO1 is normally expressed only in a restricted set of cells, including placental endothelial cells and mature dendritic cells. Studies in mice demonstrated the key role of placental IDO1 to prevent immune rejection of the fetus (7, 8). IDO1 expression in mature dendritic cells is believed to contribute to the retro-control of immune responses (9). In line with this function is the fact that IDO1 expression can be induced in most tissues and cell types upon exposure to IFNγ (10, 11). Because IFNγ is produced by T lymphocytes at the peak of their response, the ensuing induction of IDO1 ensures a negative feedback of the T-cell response. Indeed, IDO1-deficient mice develop exacerbated autoimmune pancreatitis triggered by the injection of Freund's adjuvant (12).

The availability of small-molecule inhibitors able to block IDO1 enzymatic activity allowed confirmation of the immunosuppressive role of tumor IDO1: in a number of preclinical models, the inhibition of IDO1 activity resulted in antitumor effects that were synergistic with various immunotherapy approaches, including vaccination and checkpoint blockade

[1]Ludwig Institute for Cancer Research, Brussels, Belgium. [2]de Duve Institute, Université catholique de Louvain, Brussels, Belgium. [3]Walloon Excellence in Life Sciences and Biotechnology, Brussels, Belgium.

Note: Supplementary data for this article are available at Cancer Immunology Research Online (http://cancerimmunolres.aacrjournals.org/).

Corresponding Author: Benoît J. Van den Eynde, Ludwig Institute for Cancer Research, de Duve Institute (Université catholique de Louvain), Avenue Hippocrate 74 B1.74.03, Brussels B-1200, Belgium. Phone: 32-2-764-7572; Fax: 32-2-764-7590; E-mail: benoit.vandeneynde@bru.licr.org

doi: 10.1158/2326-6066.CIR-16-0400

Published OnlineFirst July 21, 2017; DOI: 10.1158/2326-6066.CIR-16-0400

(13, 14). In a wide range of human tumors, IDO1 expression was also correlated with a worse prognosis and a reduced T-cell infiltration (15–17). These results have prompted the clinical development of IDO1 inhibitors, which are now in phase III trials.

Although mouse studies highlighted increased IDO1 expression in tumor-draining lymph nodes, this was not observed in humans (9). In addition, mechanistic studies indicated that the relevant IDO1 for tumor-induced immune suppression was present at the tumor site (18). There are distinct patterns of IDO1 expression in human tumors (9). A number of tumors show IDO1 expression associated with a T-cell infiltrate and signs of inflammation. This expression likely results from induction by IFNγ produced by infiltrating T cells. Such a pattern of expression, indicative of adaptive immune resistance, has been observed for other immune counter-regulatory molecules such as PD-L1 (19). In contrast, many human tumors express IDO1 in the absence of any inflammation and T-cell infiltrate, representing a state of intrinsic immune resistance (3, 9). This may account for the clinically relevant group of "cold" or "noninflamed" tumors, which fail to respond to checkpoint inhibitors due to the lack of T-cell infiltrate. This pattern of IDO1 expression is recapitulated in a number of human tumor cell lines that express IDO1 in a constitutive manner, i.e., in the absence of IFNγ (13). Little is known about the signaling mechanisms accounting for constitutive IDO1 expression in human tumors.

Here, we report the characterization of the signaling pathways accounting for constitutive IDO1 expression in a series of human tumor cell lines. Our results show that autocrine prostaglandin E_2 triggers PKC and PI3K signaling, which in turn leads to IDO1 transcription. PGE_2 production results from constitutive expression of COX-2 triggered by MAPK signaling. These tumors harbor oncogenic mutations in one or several of these signaling pathways, which likely contribute to constitutive IDO1 expression making up an immunosuppressive tumor phenotype. Blocking COX-2 activity *in vivo* prevents IDO1 expression and restores immune rejection of human tumors in a mouse model reconstituted with human lymphocytes. Our results provide a mechanistic explanation for the reported role of COX-2 in tumor evasion of immunity (20–22). Our results also highlight a link between oncogenic signaling and immunosuppression in human tumors and suggest the use of COX-2 inhibitors as immune modulators to increase the clinical efficacy of cancer immunotherapy.

Materials and Methods

Cancer cell lines

KUL98-MELA and KUL98-MELB are melanoma nodules that were obtained from UZ Leuven Gasthuisberg in 2003 and 2004, respectively. Authentication by DNA finger printing was last done in September 2014. *Mycoplasma* tests were done in July 2004 for KUL98-MELA and April 2005 for KUL98-MELB. LB919-SCCHN was derived at the Ludwig Institute Brussels Branch from a patient sample donated by Cliniques universitaires Saint-Luc in February 1994 and tested for *mycoplasma* in April 1994. No authentication was carried out. LB1610-MEL was derived at the Ludwig Institute Brussels Branch from a patient sample donated by Cliniques universitaires Saint-Luc in July 1997 and last tested for *mycoplasma* in November 2012. Authentication was last carried out in May 2011 by DNA finger printing. LB188-SAR was derived at the Ludwig Institute Brussels Branch from a sample donated by Hôpital Jolimont in May 1991 and last tested for *mycoplasma* in January 1992. No authentication was done. LS411N was received from collaborators in Lausanne in 1990. Neither *mycoplasma* test nor authentication has been done. NCI-H596 was purchased from the ATCC in 1995 and last tested for *mycoplasma* in November 2012. No authentication has been carried out. U87 was purchased from CLS Cell Lines Services GmbH in 2011. Neither *mycoplasma* test nor authentication has been done. A172 was purchased from Antisense Pharma GmBH in 2004 and last tested for *mycoplasma* in November 2012. No authentication has been carried out. MZ-CHA-3 was received from collaborators in Mainz in 1991 and last authenticated in May 2011 by DNA finger printing. No *mycoplasma* test has been done. SKOV3 was purchased from CLS Cell Lines Services GmbH in 2014 and last authenticated by DNA finger printing in August 2016. No *mycoplasma* test has been done. Cells were cultured under standard conditions. For PGE_2 metabolite quantification, cells were cultured in X-VIVO 15 medium (Lonza). All *mycoplasma* tests were done by qPCR.

Compounds

LY294002 (4402-4) (used at 20 μmol/L for 24 hours) and R0-31-8425 (557514) (20 μmol/L for 24 hours) were obtained from Calbiochem. GDC0941 (957054-33-0) (5 μmol/L for 72 hours) was bought from Axon Medchem. A66 (S2636) (20 μmol/L for 72 hours), TGX221 (S1169) (30 μmol/L for 72 hours), MK2206 (S1078) (10 μmol/L for 72 hours), and ruxolitinib (S1378) were bought from Selleckchem. CAY10598 (13281) (10 μmol/L for 24 hours) was obtained from Cayman Chemicals. H-89 (B1427) and rapamycin (R3781) (200 nmol/L for 8 hours) were bought from Sigma. PLX4032 (S1267)(10 μmol/L for 72 hours) was bought from Selleckchem. U0126 (BML-EI282-0001) (20 μmol/L for 72 hours), and SB203580 (EI-286-0005) (10 μmol/L for 72 hours) were obtained from ENZO. Celecoxib (used at 5 μg/mL) was bought by prescription from Pfizer. MF63 (10 μmol/L) was bought from AbMole BioScience. AH6809 (14050), GW627368X (10009162) both used at 10 μg/mL were obtained from Cayman Chemicals. Celecoxib, MF63, AH6809, and GW627368X were added twice (days 0 and 2) on a 3-day period. Epacadostat was obtained from Chemietek. Human recombinant IL1β (200-01B) (1 μg/mL for 12 hours) and human IFNγ (300-02) were bought from Peprotech. Anakinra (Kineret 10 mg/0.67 mL), used at 50 μg/mL for 72 hours, was bought by prescription from Sobi.

Western blot

Cells were lysed in homemade lysis buffer [0.1% SDS, 1% deoxycholic acid, 0.5% NP40 complemented with protease and phosphatase inhibitors (Roche)]. Proteins were separated on precast NuPage 4% to 12% Bis-Tris gels (Invitrogen) in MOPS running buffer. Dry transfer was done with the iBlot from Thermo Scientific. Membranes were blocked in PBS or TBS containing 5% dry milk and 0.1% Tween 20 and then probed with the primary antibodies at 4°C overnight. Images were acquired by Fusion Fx camera from Vilber Lourmat. Quantification was obtained with the Bio-1D (version 15.06b) software from Vilber Lourmat.

p-AKT (Ser 473) rabbit mAb (#4060 from Cell Signaling Technology), AKT rabbit mAb (#4691 from Cell Signaling Technology), p-GSK3β (Ser9) rabbit mAb (#5558 from Cell Signaling Technology), GSK3β mouse mAb (#9832 from Cell Signaling Technology), p-p70S6K (T389) rabbit mAb (#9234 from Cell

Published OnlineFirst July 21, 2017; DOI: 10.1158/2326-6066.CIR-16-0400

Signaling Technology), p70S6K rabbit mAb (#2780 from Cell Signaling Technology), p-CREB (Ser133) rabbit mAb (#9191 from Cell Signaling Technology), CREB rabbit mAb (#9197 from Cell Signaling Technology), p-p44/42 MAPK (ERK1/2) (Thr202/Tyr204) rabbit mAb (#4370 from Cell Signaling Technology), p44/42 MAPK rabbit polyclonal Ab (#9102 from Cell Signaling Technology), β-catenin rabbit mAb (#8480 from Cell Signaling Technology), p-STAT3 (Y705) rabbit mAb (#9145 from Cell Signaling Technology), STAT3 rabbit mAb (#4904 from Cell Signaling Technology), p-STAT1 (Tyr 701) rabbit polyclonal Ab (#9171 from Cell Signaling Technology), and STAT1 rabbit polyclonal Ab (#9172) were diluted at 1/1,000. IDO1 mouse antibody (4.16H1 clone 7) was homemade and used at 2 μg/mL (9). Actin mouse antibody (A5441) bought from Sigma was used at 1/10,000. Vinculin mouse mAb (hVIN-1) antibody (V9131) bought from Sigma was used at 1/2,000.

Secondary antibodies were incubated 1 hour at room temperature before revelation with the cheluminescent substrate West Pico SuperSignal sold by Thermo Scientific. Anti-rabbit HRP-linked IgG (#7074 from Cell Signaling Technology) was used at 1/3,000, and anti-mouse HRP-conjugated IgG (HAF007 from R&D Systems) was used at 1/5,000.

qPCR

RNA was extracted by Tripure (Roche), and the retro-transcription was done with the revertAid kit from Thermo Scientific (K1691). RT-qPCR was performed with the Takyon Rox probe core kit dTTP from Eurogentec (UF-RPCT-C0201). RT-qPCR for *IDO1* (Forward: GGTCATGGAGATGTCCGTAA; Reverse: ACCAATAGAGAGACCAGGAAGAA; Probe: CTGTTCCTTACTGTCAACTCTCCAAGAAACTG), *mPGES1* (F: GCTGGTCATCAAGATGTACG; R: CCAGGTAGGCCACGGTGTCT), *EP2* (F: CCACCTCATTCTCCTGGCTA; R: CGACAACAGAGGACTGAACG), *EP4* (F: TGGTATGTGGGCTGGCTG; R: GAGGACGGTGGCGAGAAT), and *GAPDH* (F: TCAACGACCACTTTGTCAAGC; R: CCAGGGGTCTTACTCCTTGG; Probe: CCTGGTATGACAACGAATTTGGCTACAGC) was performed with an elongation condition of 62°C for 1 minute. RT-qPCR for *COX-2* (F: CAGGCTAATACTGATAGGAGAGA; R: TTGACAACTATCAACATAAAGACCAGT), *EP1* (F: GGTATCATGGTGGTGTCGTG; R: GGCCTCTGGTTGTGCTTAGA), *EP3* (F: CTTCGCATAACTGGGGCAAC; R: TCTCCGTGTGTGTCTTGCAG), *IL1β* (F: CTGCCCACAGACCTTCCA; R: GGACCAGACATCACCAAGC; Probe: AATGACCTGAGCACCTTCTTTCCTT), *IL8* (F: CTGAGACTGATTGAGAGTGGA; R: GTGTTGAAGTAGATTTGCTTGAAG; Probe: AGCTCTGTCTGGACCCCAAGGAAAAC) *CD3*ε (F: GGCAAGATGGTAATGAAGAAATGG; R: AGGGCATGTCAATATTACTGTGGTT), *CD8β* (F: CAGCTGAGTGTGTGGTTGATTTCC; R: ACCGGCACACTCTCTTCTTGA; Probe: CCCACCACTGCCCAGCCCAC), and *Actin* (F: GGCATCGTGATGGACTCCG; R: GCTGGAAGGTGGACAGCGA; Probe: TCAAGATCATTGCTCCTCCTGAGCGC) was performed with an elongation condition of 60°C for 1 minute.

Mouse experiments

NSG mice (from The Jackson Laboratory) were bred at the animal facility of the Ludwig Institute for Cancer Research, Brussels, Belgium. Handling of mice and experimental procedures were conducted in accordance with national and institutional guidelines for animal care. NSG mice were injected subcutaneously with 4×10^6 SKOV3 or LS411N cells. After 7 days (d-3), the tumors were measured and randomized groups of mice (9 for SKOV3 and 8 for LS411N) were treated or not with celecoxib (10 mg/kg once a day) and/or IDO1 inhibitor epacadostat (100 mg/kg twice a day) by oral gavage (d-3). Control mice received methocel (100 μL). Three days later (d0), the mice were injected or not with 3×10^6 human allogeneic peripheral blood mononuclear cells (PBMC; d0) in the tail vain. Under those conditions, mice did not develop graft-versus-host disease (GVHD) before day 40. Tumors were measured at regular intervals with an electronic caliper. Mice were sacrificed after 40 days and tumors were resected and frozen for immunochemistry, RNA, and protein extraction. RNA and proteins were extracted after crushing the tumors in liquid nitrogen.

Isolation of PBMCs

PBMCs were purified from the blood of a hemochromatosis donor (LB2419), courtesy of Saint-Luc University Hospital, by centrifugation on a Lymphoprep gradient and then frozen at −80°C.

Lentivirus production and transduction of target cells

Recombinant lentiviruses were produced by transient cotransfection of 293T cells in 100-mm tissue culture dishes with 4.2, 2.1, and 2.5 μg of pGAG-POL, pREV, and PVSV-G, respectively, for viral encapsidation. At the same time, the shSTAT3 pGIPZ vector (V3LHS_641817 from Dharmacon) or the pGIPZ empty vector (RHS4351 from Dharmacon) was transfected too. The transfection was performed using the calcium phosphate precipitation method. The medium was replaced 4 hours later and virus-containing supernatants were harvested after 24, 48, and 72 hours after transfection. Cancer cells were then plated in a 6-well plate and 500 μL of viral supernatant and 500 μL of fresh media were added after 4 hours. Seventy-two hours later, supernatants were discarded and fresh media were added with 3 μg/mL of puromycin for selection.

Tryptophan and kynurenine quantification

Cells were treated with 5 μg/mL of celecoxib or 10 μg/mL of GW627368X every 2 days, 20 μmol/L LY294002 or 10 μmol/L MK2206, 20 μmol/L Ro-31-8425, or 10 μmol/L SB203580 every 3 days. Cell culture supernatants were harvested up to 7 days after plating and analyzed by HPLC as previously described (23). Time point 0 corresponds to cell-free medium.

PGE_2 metabolite detection assay

Cells were cultured in X-VIVO 15 medium (Lonza) for 5 days before supernatants were collected and PGE_2 metabolites (13,14-dihydro-15-keto PGA_2 and 13,14-dihydro-15-keto PGE_2) quantified by a prostaglandin E metabolite EIA kit from Cayman Chemical. Control corresponds to cell-free X-VIVO 15 medium.

Quantification of IL1β

KUL98-MELA and KUL98-MELB cells were cultured in X-VIVO 15 medium for 3 days. The supernatant was harvested, and IL1β was quantified with the human IL1β ELISA Ready-SET-Go from Affymetrix-eBioscience (88-7261-88).

siRNA

siRNA (100 nmol/L) directed against *CTNNB1* and the negative control siRNA diluted in Opti-MEM medium (ThermoFisher Scientific) were first incubated with lipofectamin 2000 (Invitrogen) before adding the lipofectamin-siRNA mixture on the cancer

Published OnlineFirst July 21, 2017; DOI: 10.1158/2326-6066.CIR-16-0400

cells for 6 hours. The medium was changed after 6 hours, and cells harvested after 48 hours were analyzed. *CTNNB1* Silencer validated siRNA (AM51331) and Silencer Negative Control siRNA (AM4611) were purchased at Ambion ThermoFisher Scientific.

RNAseq

RNA samples were prepared from cell lines using the guanidinium isothiocyanate/cesium chloride procedure (24). Mutations in KUL98-MELA, KUL98-MELB, MZ-CHA-3, and LB1610-MEL cell lines were visually detected in selected genes from RNAseq data performed on an in-house SOLID platform. Mutations in LB188-SAR and LB919-SCCHN cell lines were visually detected in selected genes from RNAseq data performed on an Illumina TrueSeq platform. Coverage was of 470M reads (2 × 125 bp paired end) at Beckman Coulter Inc.

Cancer cell line encyclopedia

Expression data and mutation data were extracted from the Cancer Cell Line Database from the Broad Institute in collaboration with Novartis. The database was validated by quantifying *IDO1* expression by RT-qPCR in a series of cancer cell lines available at the Ludwig Institute. Significance of the comparisons between the *IDO1*-positive and *IDO1*-negative populations was assessed by unpaired *t*-test with Welch correction (unequal variance, *F* test was significant). Correlation between *IDO1* and *COX-2* or *mPGES1* was evaluated by a Spearman correlation test. The differences in proportions between *IDO1*-positive mutated cell lines and *IDO1*-positive nonmutated cancer cell lines were tested by a unilateral Fisher test. The mutations taken in account for this study were mined from the CCLE database and located in oncogenic hotspots: *PI3K*, *AKT*, *PTEN*, *HRAS*, *BRAF*, *NRAS*, and *KRAS*.

SKOV3 and lymphocyte proliferation

On day 0, SKOV3 cells were plated in a 96-well flat bottom plate and treated with different concentrations of epacadostat. Human allogeneic PBMCs (LB2419) were stimulated with $CD3^+/CD28^+$ beads and IL2 for 10 minutes before coculturing them with SKOV3 cells at a 1:2 SKOV3/PBMC ratio. On day 1, supernatants were harvested for tryptophan/kynurenine quantification assay by HPLC and ^{3}H-thymidine was added in each well. On day 2, PBMC proliferation was measured by thymidine incorporation (TopCount counter Perkin Elmer). In a separate experiment, human allogeneic PBMCs (LB2419) prestimulated with $CD3^+/CD28^+$ beads and IL2 for 10 minutes were cultivated either in fresh medium supplemented or not with celecoxib 5 μg/mL, or in conditioned medium from SKOV3 cells cultured 72 hours in the presence or absence of celecoxib 5 μg/mL. On day 1, ^{3}H-thymidine was added and PBMC proliferation was measured as above. On day 2, the supernatants were also used to quantify the Th1 and Th2 cytokines with the Bio-Plex Pro Human cytokine Th1/Th2 assay from Bio-Rad.

Immunohistochemistry

Tumors were extracted at the end point of each experiment and frozen. Frozen sections (5 μm) were incubated 5 minutes in 4% formaldehyde for fixation. Endogenous peroxidases were blocked with DAKO peroxidase blocking solution for 15 minutes, and nonspecific staining was prevented by incubation in a 5% BSA, 2% milk, and 1% human IgG solution in TBS-T for 1 hour. Sections were then incubated with a 1/200 dilution in REAL antibody diluent (#S2022 from Agilent) of the rabbit anti-human CD3 antibody (Clone SP7, # ab16669 from Abcam, concentration 1–3 mg/mL) or 1/200 dilution of the mouse anti-human CD8 antibody (Clone C8/144B, #M710301 from Agilent, concentration 157 mg/L). The anti-mouse goat polymer HRP (#K4005 from Agilent) or the anti-rabbit goat polymer-HRP (#K4009 from DAKO) was then added and incubated for 1 hour. Finally, sections were stained with the AEC+ chromogenic substrate (#K4005 from Agilent) for 20 minutes and counterstained with a solution of hematoxylin for 5 minutes. Stained sections were digitalized with a Pannoramic P250 Flash III slide scanner (3DHISTECH) and were analyzed with CaseViewer (3DHISTECH). Sections were quantified with the ImageJ software.

Statistical method

For the analysis of the effect of the different inhibitors, an unpaired *t*-test was done; the Welch correction was applied in the cases where the variance was not equal. The *P* values are annotated as follows: *, $P < 0.05$; **, $P < 0.01$; ***, $P < 0.005$; and ****, $P < 0.0001$. For the mouse *in vivo* experiments, a nonparametric "Anova Wilcoxon each pairs" test was done on the last time point.

Results

Autocrine PGE_2 drives IDO1 expression in human melanoma

We selected a series of human cancer cell lines that constitutively express IDO1 and, accordingly, degrade tryptophan and produce kynurenine in equimolar amounts (13) (Supplementary Table S1). We focused our initial experiments on a *BRAF* V600E-mutated melanoma cell line, named KUL98-MELA. Because IFNγ induces IDO1 expression, we first considered the possibility that KUL98-MELA might display a constitutive activation of the IFNγ signaling pathway, which entails JAK1/JAK2-mediated phosphorylation of STAT1. We observed that ruxolitinib, a JAK1/JAK2 inhibitor, did not reduce the constitutive levels of *IDO1* transcripts in KUL98-MELA cells (Supplementary Fig. S1A), although it prevented both IDO1 induction and STAT1 phosphorylation triggered by addition of IFNγ (Supplementary Fig. S1B). These results indicated that constitutive IDO1 expression was not triggered by the IFNγ signaling pathway in these melanoma cells.

COX-2 shapes the immunosuppressive tumor microenvironment of mouse melanoma, although the downstream mechanisms remain unclear (20). In addition, PGE_2 contributes to induction of IDO1 expression in dendritic cells during the maturation process (25). These observations prompted us to consider that the PGE_2 signaling pathway might be involved in constitutive IDO1 expression by human tumor cells. We observed that celecoxib, a COX-2 specific inhibitor, reduced the levels of *IDO1* transcripts by 3-fold in KUL98-MELA cells (Fig. 1A). Moreover, the IDO1 protein was not detectable in treated cells, which no longer degraded tryptophan nor produced kynurenine (Fig. 1A and B). As another means of preventing PGE_2 formation, we then used MF63, an inhibitor of membrane-associated PGE_2 synthase (mPGES1), and observed again a reduction of *IDO1* transcripts and protein levels (Fig. 1A). We then considered that PGE_2 might trigger autocrine signaling and investigated the expression of the four isoforms of PGE_2 receptors, EP1-4, on our melanoma cells. We observed expression of *EP4* transcripts (Fig. 1C). We therefore inhibited EP4 with a competitive antagonist, GW627368X, and observed again a decrease in *IDO1* transcripts, IDO1 protein, and

Published OnlineFirst July 21, 2017; DOI: 10.1158/2326-6066.CIR-16-0400

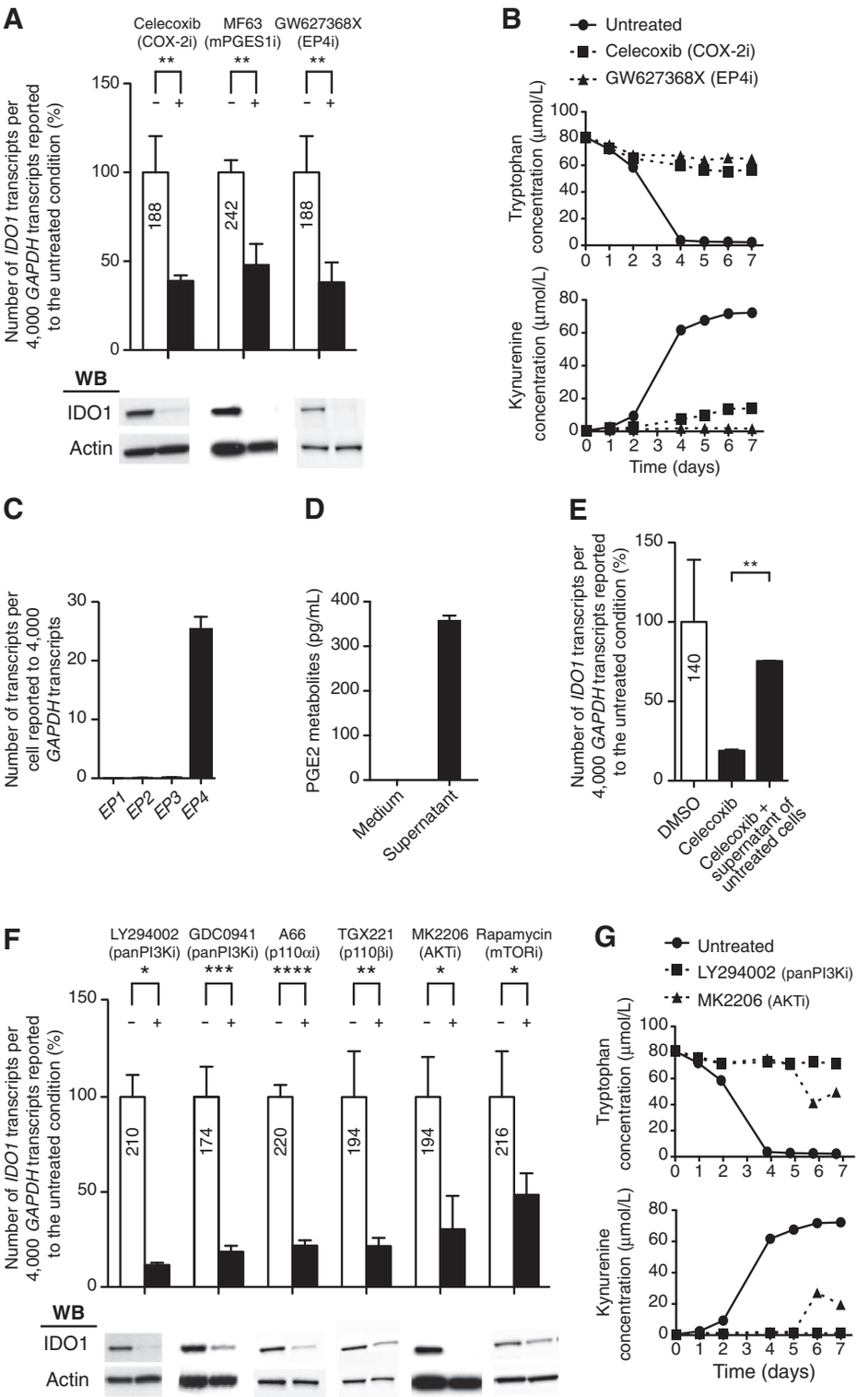

Figure 1.

Involvement of the PGE_2 and PI3K pathways in constitutive *IDO1* expression. **A,** KUL98-MELA cells were treated for 3 days with different inhibitors of the PGE2 pathway, RT-qPCR, and Western blot analysis were then performed. The number of IDO1 transcripts was reported to that of the untreated cells, and the absolute number of transcripts in the untreated cells is indicated on the histogram. This representation is used throughout the manuscript. **B,** Tryptophan and kynurenine concentrations were measured by HPLC. **C,** Quantification by RT-qPCR of EP receptor transcripts was performed on RNA extracted from KUL98-MELA cells. **D,** PGE_2 metabolite levels were measured in supernatant from KUL98-MELA cells. **E,** KUL98-MELA cells were treated with celecoxib for 4 days. Every day the culture medium was replaced with fresh X-VIVO medium or with 24 h-culture supernatant of untreated KUL98-MELA cells, both containing fresh celecoxib. **F,** KUL98-MELA cells were treated with PI3K pathway inhibitors before RT-qPCR and Western blot analysis. **G,** Tryptophan and kynurenine concentrations were measured by HPLC. Mean + SD of triplicates from one out of three experiments. See also Supplementary Figs. S1 and S2.

enzymatic activity in the treated melanoma cells (Fig. 1A and B). Altogether, these results suggested that constitutive IDO1 expression in KUL98-MELA cells was triggered by an autocrine loop of PGE_2 secretion. In line with this, we observed the production of up to 400 pg/mL of PGE_2 metabolites in the culture supernatant of those cells (Fig. 1D). Moreover, addition of this PGE_2-containing supernatant to celecoxib-treated KUL98-MELA cells restored *IDO1* expression by these cells (Fig. 1E).

Published OnlineFirst July 21, 2017; DOI: 10.1158/2326-6066.CIR-16-0400

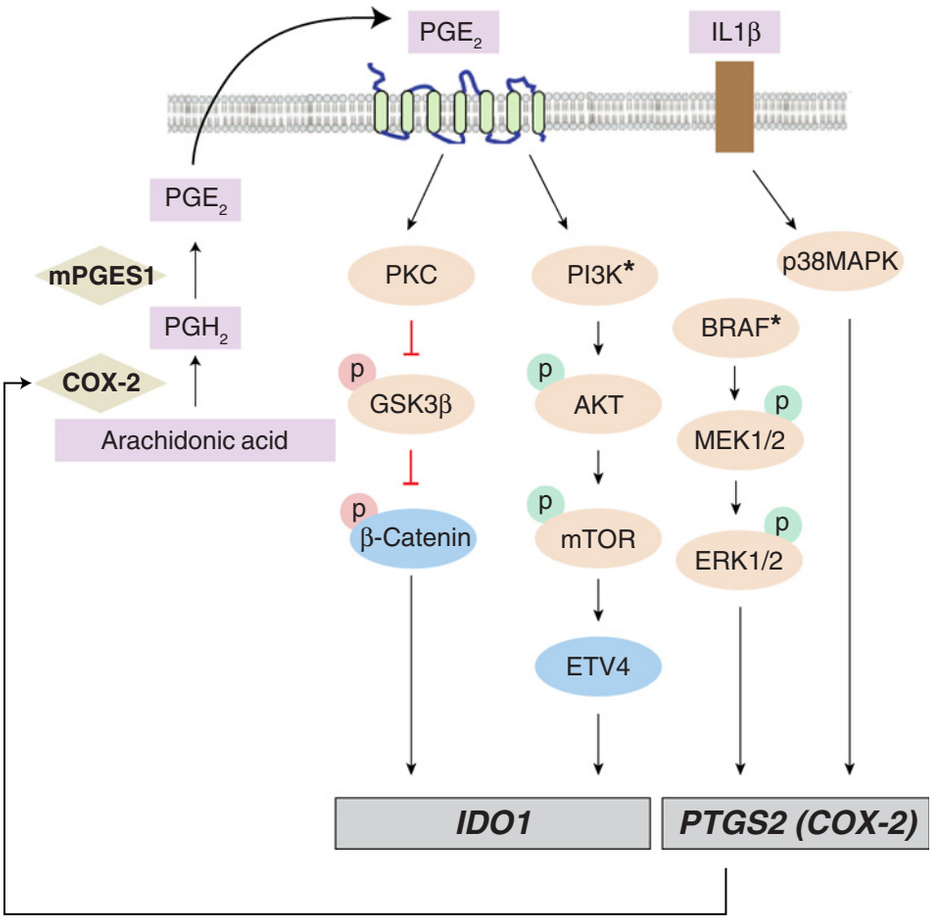

Figure 2.
Signaling pathway responsible for constitutive IDO1 expression in human cancer cells. The asterisk denotes potential mutation sites that contribute to constitutive expression of IDO1. *PTGS2* is the gene encoding COX-2. Green phosphorylation symbols in the PI3K/AKT and MAPK pathways indicate an activating process. Red phosphorylation symbols indicate an inactivating process such as the phosphorylation of serine 9 of GSK3β by PKC and the phosphorylation of β-catenin by the active form of GSK3β, resulting in β-catenin degradation by the proteasome.

Involvement of the PI3K and PKC signaling pathways

To characterize the link between PGE_2 signaling and IDO1 expression, we investigated the signaling pathways downstream of the EP receptors, which are G protein–coupled receptors able to activate the PKA, PI3K, and PKC pathways (26–28).

H-89, a competitive inhibitor of PKA, did not reduce *IDO1* transcript levels in KUL98-MELA cells, although it reduced phosphorylation of PKA downstream effector CREB (Supplementary Fig. S1C).

In contrast, LY294002, a pan-PI3K inhibitor, reduced *IDO1* transcript levels and abolished both IDO1 protein expression and enzymatic activity (Fig. 1F and G). Similar results were obtained using GDC-0941, a pan-PI3K inhibitor used in clinical trials (ref. 29; Fig. 1F). PI3K-subunit specific inhibitors A66 (p110α inhibitor) and TGX221 (p110β inhibitor) also reduced *IDO1* transcript levels (Fig. 1F). All these inhibitors effectively reduced phosphorylation of AKT, a downstream effector of the PI3K pathway (Supplementary Fig. S2A–S2D). MK2206, an AKT inhibitor, also reduced IDO1 expression and enzymatic activity (Fig. 1F and G). Because AKT can phosphorylate both GSK3β and p70S6K, we assessed the phosphorylation of these proteins in treated cells. Although p70S6K phosphorylation was abrogated by MK2206 treatment, GSK3β phosphorylation was not affected (Supplementary Fig. S2E). We observed similar results with the different PI3K inhibitors (Supplementary Fig. S2A–S2D). These results suggested that, although EP receptors signal through the PI3K pathway, this pathway is not involved in GSK3β phosphorylation, but rather activates mTOR, consistent with the fact that p70S6K phosphorylation is abrogated by all the PI3K and AKT inhibitors. This was confirmed by treatment of KUL98-MELA cells with rapamycin, which led to reduction of IDO1 expression (Fig. 1F) and abrogation of phospho-p70S6K (Supplementary Fig. S2F). We suggest a possible signaling pathway for constitutive IDO1 expression in human tumors in Fig. 2.

Finally, we tested the PKC pathway, which can inactivate GSK3β by phosphorylating its serine 9 in the same manner as PI3K (30). Upon treatment with pan-PKC inhibitor Ro-31-8425, KUL98-MELA cells reduced their IDO1 expression and enzymatic activity and dephosphorylated GSK3β (Fig. 3A–C). GSK3β regulates a number of transcription factors, including β-catenin, which binds the *IDO1* promoter (30, 31). Silencing β-catenin with siRNA reduced levels of IDO1 transcript and protein (Fig. 3D). We confirmed this PKC pathway to be independent from the PI3K/AKT pathway described above, by testing a combination of the AKT inhibitor MK2206 and the pan-PKC inhibitor Ro-31-8425: we observed an additive inhibitory effect on IDO1 expression, indicating that both pathways act independently downstream of the EP4 receptor (Fig. 3E). Altogether, we conclude that PGE_2-triggered signaling involves both the PKC pathway, which activates IDO1 via β-catenin, and the PI3K pathway, which activates IDO1 via mTOR. The mTOR activation may depend on the transcription factor ETV4/PEA3, which functions downstream

Published OnlineFirst July 21, 2017; DOI: 10.1158/2326-6066.CIR-16-0400

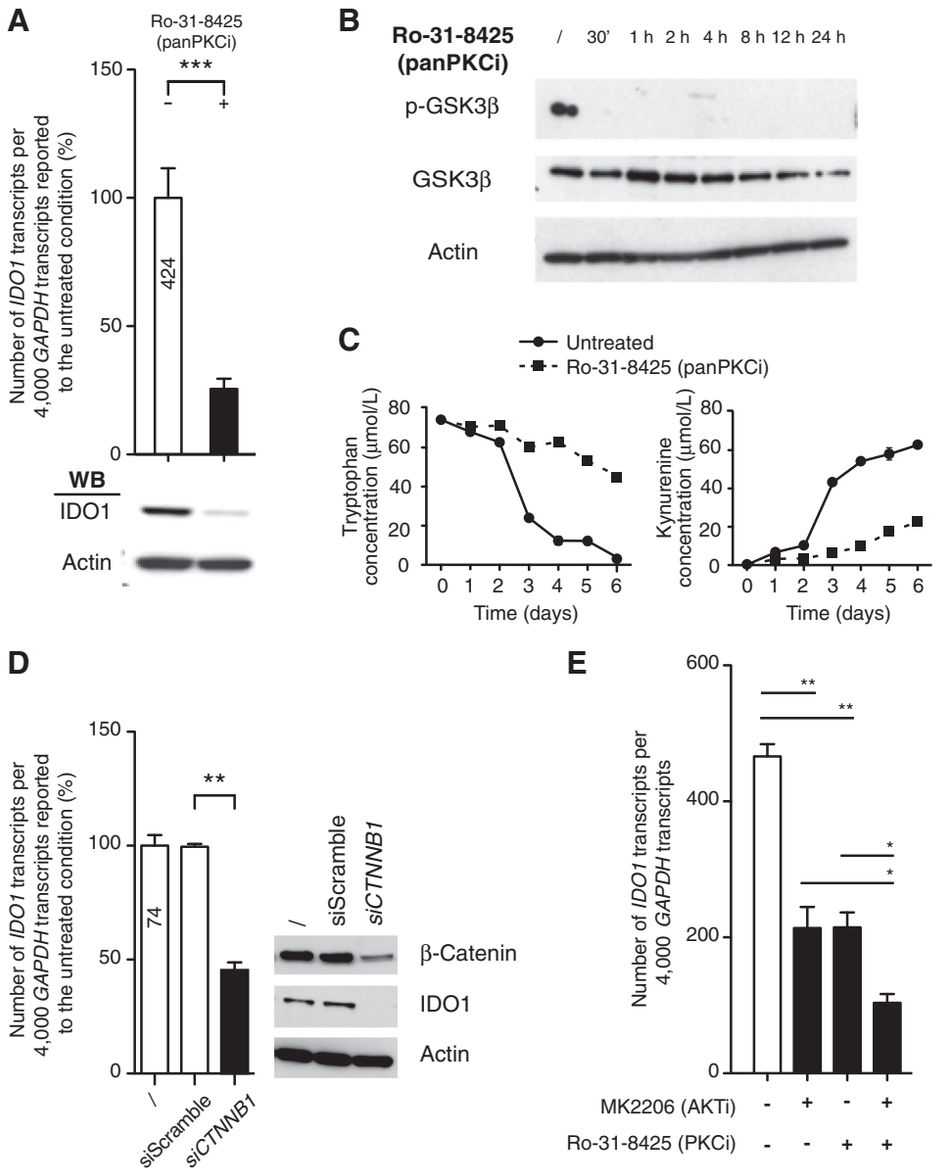

Figure 3.

Involvement of the PKC pathway. **A,** KUL98-MELA cells were treated with a pan-PKC inhibitor before RT-qPCR and Western blot analysis. **B,** KUL98-MELA cells treated for the indicated times were analyzed by Western blot. **C,** Tryptophan and kynurenine concentrations were measured by HPLC. **D,** β-catenin was silenced by siRNA (*CTNNB1*) in KUL98-MELA cells and Western blot analysis was performed. **E,** KUL98-MELA cells were incubated 72 hours with MK2206, 24 hours with Ro-31-8425 or 72 hours with MK2206 supplemented with Ro-31-8425 after 48 hours and expression of *IDO1* was analyzed by RT-qPCR. Mean + SD of triplicates from one out of three experiments.

of mTOR and binds the *IDO1* promoter (32) (Fig. 2). Of note, melanoma-intrinsic β-catenin signaling was found to be linked to immune evasion and resistance to immunotherapies (33).

Activated MAPK pathways support constitutive COX-2 expression

Because KUL98-MELA cells harbor a *BRAF* V600E mutation, we also investigated the role of the MAPK pathway in constitutive IDO1 expression. We used a *BRAF* V600E inhibitor (PLX4032), a MEK1/2 inhibitor (U0126) and a p38MAPK inhibitor (SB203580). All reduced IDO1 expression in KUL98-MELA cells (Fig. 4A and B). Because the expression of *COX-2* is also controlled by the ERK1/2 pathway, we also measured COX-2 expression and found that it was reduced in cells treated with these inhibitors (34) (Fig. 4C). In contrast, the PGE_2 and PI3K pathway inhibitors we used above did not reduce *COX-2* expression (Supplementary Fig. S3). Altogether, these results suggest an indirect involvement of the MAPK pathway in constitutive IDO1 expression, ensuring constitutive expression of COX-2 to sustain autocrine production of PGE_2 (Fig. 2).

Autocrine IL1β supports PGE_2 production and IDO1 expression

KUL98-MELB is another melanoma line derived from a different metastasis from the same patient. KUL98-MELB cells do not express IDO1. As compared to KUL98-MELA cells, they express COX-2 at a similar level, but mPGES1 at a much lower level (Fig. 5A). Accordingly, they produce no PGE_2 (Fig. 5B), likely explaining why they do not express IDO1. To understand why KUL98-MELB cells express less mPGES1 than KUL98-MELA, we considered IL1β, which can control expression of both COX-2 and mPGES1, and we compared the expression of IL1β and its target gene *IL8* (35–37). We observed that KUL98-MELB cells expressed less of *IL1β* and *IL8* transcripts (Fig. 5C and D) and produced less

Published OnlineFirst July 21, 2017; DOI: 10.1158/2326-6066.CIR-16-0400

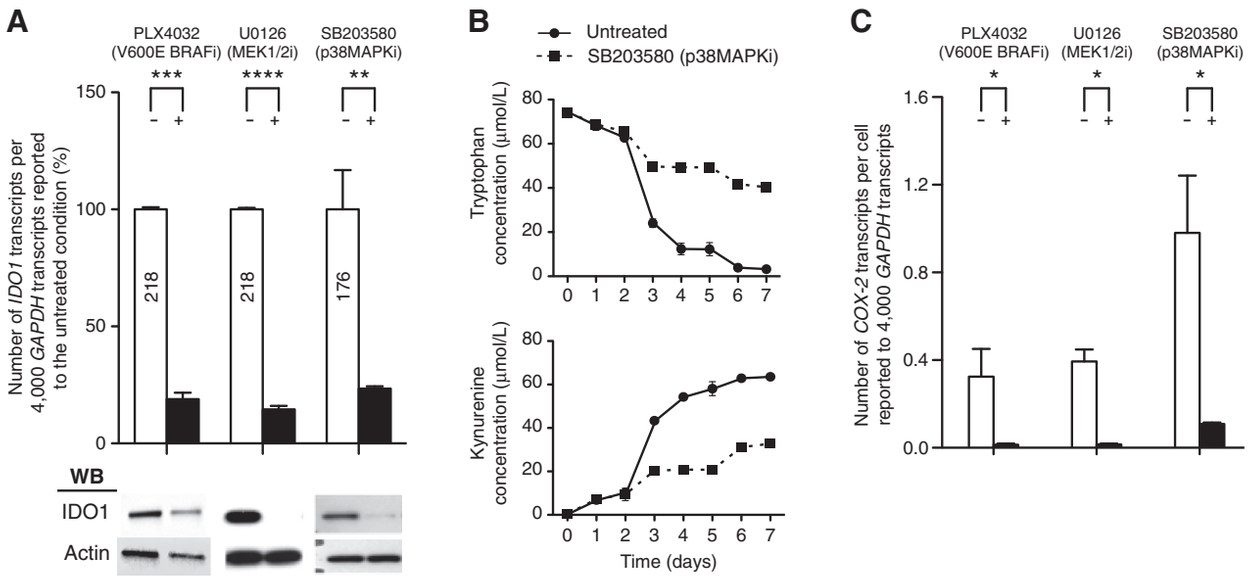

Figure 4.

Involvement of the MAPK pathway. **A,** KUL98-MELA cells were treated with MAPK pathway inhibitors for 3 days before RT-qPCR and Western blot analysis. **B,** Tryptophan and kynurenine concentrations were measured by HPLC. **C,** The same extracts as in **A** were used to quantify the transcripts of *COX-2* by RT-qPCR. Mean + SD of triplicates from one out of three experiments. See also Supplementary Figs. S2 and S3.

IL1β in their supernatant (Fig. 5E). To determine whether this lack of IL1β production was involved in the reduced mPGES1 and IDO1 expression by KUL98-MELB cells, we treated these cells with recombinant IL1β and observed increases in *IDO1*, *COX-2*, and *mPGES1* expression (Fig. 5F). The observed IDO1 induction was blocked with the p38MAPK inhibitor SB203580, but also with the EP4 inhibitor GW627368X (Fig. 5G). Hence, IL1β contributes to COX-2 and mPGES1 expression, which in turn allows PGE_2 production and IDO1 expression. These results suggest that in KUL98-MELA cells, besides the autocrine PGE_2 loop, an IL1β autocrine loop contributes to constitutive COX-2 and mPGES1 expression and therefore indirectly supports IDO1 expression (Fig. 2). Accordingly, we observed that blocking IL1β in KUL98-MELA cells with recombinant IL1ra, anakinra, reduced expression of *IL8*, a classical IL1β target, but also reduced *IDO1* expression as well as *COX-2* and *mPGES1* expression (Fig. 5H and I).

PGE_2 supports constitutive IDO1 expression by other human cancer lines

So far we have demonstrated the importance of PGE_2 and downstream signaling pathways in the KUL98-MELA melanoma line. Next, we tested whether this mechanism also accounted for constitutive IDO1 expression in other human tumor lines, including a cholangiocarcinoma line, a head and neck carcinoma line, a sarcoma line, another melanoma line, an ovarian carcinoma line and a non–small cell lung carcinoma line (Supplementary Table S1). We observed a decrease in *IDO1* expression upon treatment of these lines with celecoxib (Fig. 6A). We also profiled the expression of the four EP receptor isoforms in the tumor lines (Supplementary Fig. S4A), and treated them with the inhibitor of the most expressed isoform. In all cases, the EP inhibitor decreased *IDO1* expression (Fig. 6B). We also observed that CAY10598, an agonist of the EP4 receptor, restored *IDO1* expression in celecoxib-treated SKOV3 cells (Fig. 6C). In addition, this agonist was able to induce low levels of *IDO1* in IDO1-negative glioblastoma cell lines A172 and U87 (Fig. 6D). Finally, we confirmed the production of PGE_2 by detecting the presence of PGE_2 metabolites in the supernatant of the 4 tumor lines that we tested (Supplementary Fig. S4B). Therefore, we conclude that the COX-2/PGE_2 pathway is responsible for constitutive IDO1 expression in a wide range of different human cancer types.

We then mined the transcriptomics data of 1,041 different human cancer cell lines from the Broad Institute, looking for correlations between *IDO1* expression and activation of the COX-2/PGE_2 axis. We first took 21 of these cell lines, measured *IDO1* expression by RT-qPCR, and matched the result with the value in the RNAseq database (Supplementary Fig. S5A). This validation allowed us to use percentile 80 as a cutoff for *IDO1* positivity, with 20% of tumor lines being positive. This was in line with our previous work showing *IDO1* expression in tumor cells in 3% to 56% of tumor samples depending of the type (9). We then clustered the database according to percentile 20/80 to separate *IDO1*-negative (below percentile 20) and *IDO1*-positive lines (above percentile 80), and interrogated *COX-2* and *mPGES1* expression. We observed more expression of *COX-2* and *mPGES1* in the *IDO1*-positive group, but no correlation with housekeeping gene *VINCULIN* (Fig. 6E). Even though the number of samples became limiting when we started analyzing the database per histological tumor type, we also observed correlations between *IDO1* and *COX-2* (*PTGS2*) or *mPGES1* (*PTGES*) expression in six different cancer histotypes (Supplementary Fig. S5B).

Most of the IDO1-expressing tumor cell lines we have characterized in this work had mutations in genes of the PI3K or MAPK pathways or of receptors leading to the activation of these pathways, such as ERBB2 (Supplementary Table S1). This suggested that activation of the PI3K pathway downstream of the EP receptors or of the MAPK pathway upstream of COX-2 expression

Published OnlineFirst July 21, 2017; DOI: 10.1158/2326-6066.CIR-16-0400

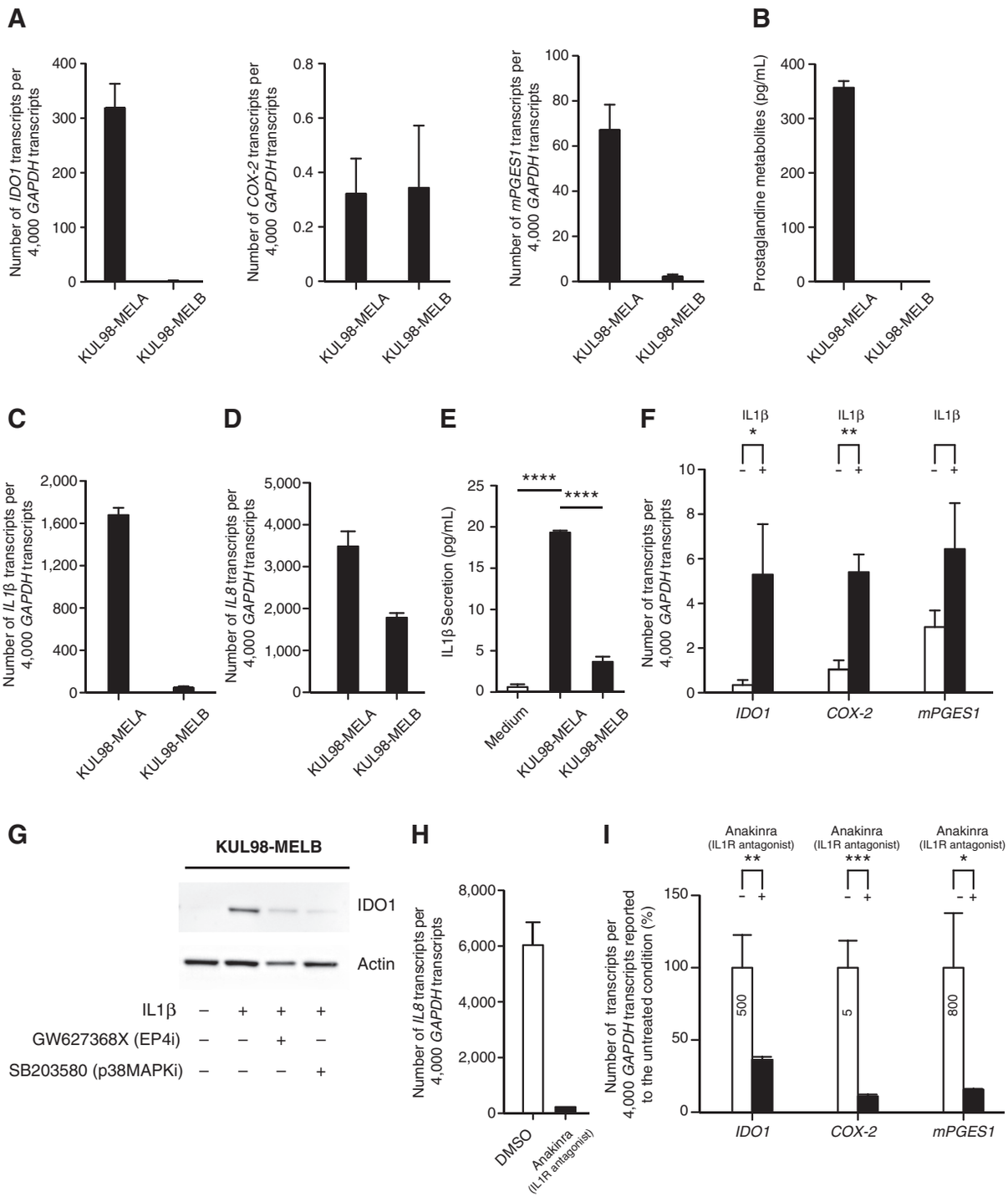

Figure 5.

Role of IL1β. **A,** RT-qPCR analysis of the expression of *IDO1, COX-2*, and *mPGES1*. **B,** PGE_2 metabolite levels were measured. **C,** RT-qPCR analysis of the expression of *IL1β*. **D,** *IL8* was quantified by RT-qPCR. **E,** Supernatants of KUL98-MELA and KUL98-MELB cells were harvested and IL1β was quantified by ELISA; fresh medium was used as a control. **F,** KUL98-MELB cells were treated with IL1β for 12 hours before RT-qPCR analysis. **G,** KUL98-MELB cells were pretreated with GW627368X or SB203580 at day 0. At day 3 the cells were treated with IL1β for 12 hours, with GW627368X or with SB203580.Western blots were then performed. **H,** *IL8* transcripts were quantified by RT-qPCR after treatment of KUL98-MELA cells with anakinra. **I,** KUL98-MELA cells were treated 72 hours with anakinra before RT-qPCR analysis. Mean + SD of triplicates from one out of three experiments.

Published OnlineFirst July 21, 2017; DOI: 10.1158/2326-6066.CIR-16-0400

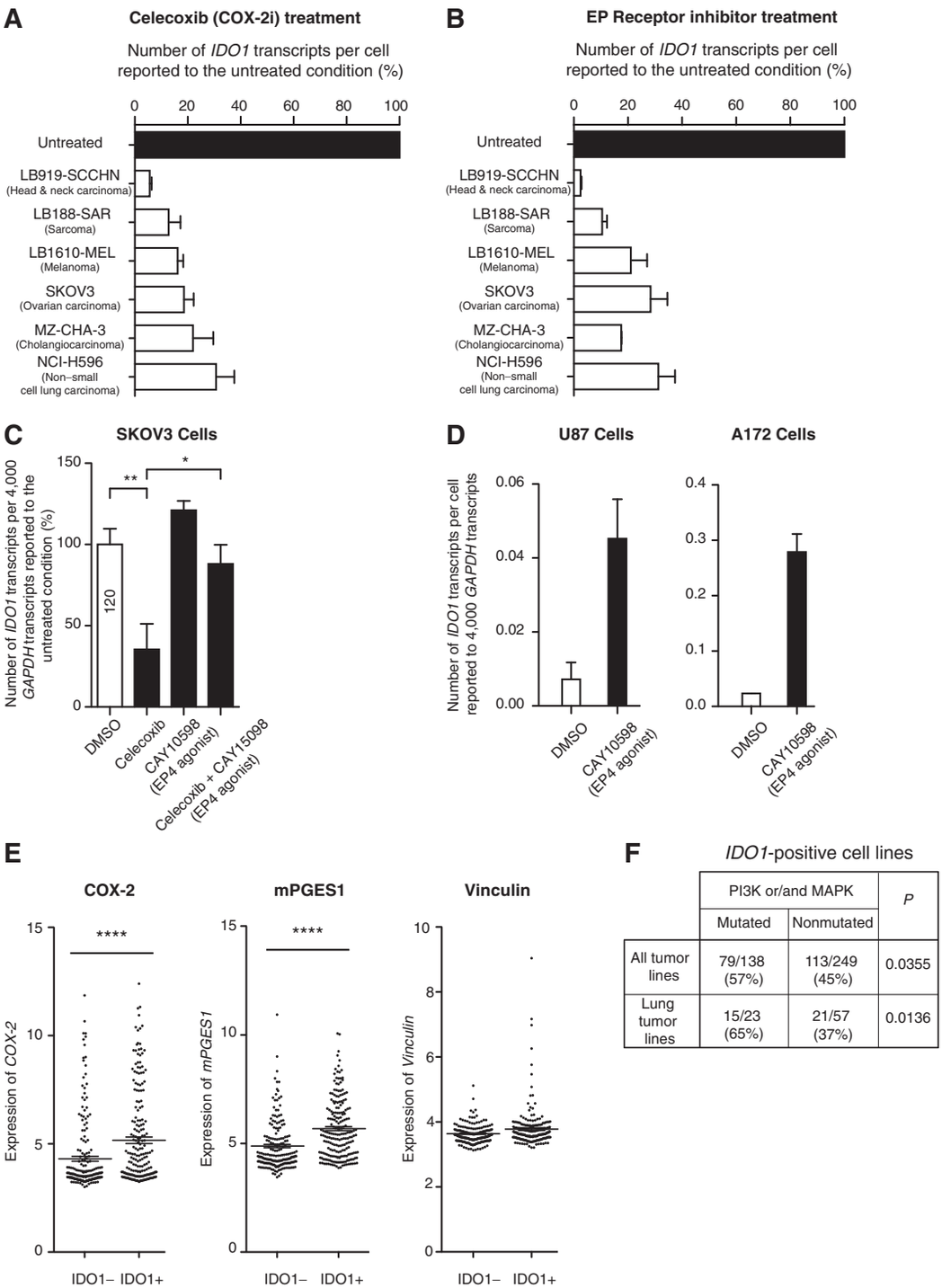

	PI3K or/and MAPK		*P*
	Mutated	Nonmutated	
All tumor lines	79/138 (57%)	113/249 (45%)	0.0355
Lung tumor lines	15/23 (65%)	21/57 (37%)	0.0136

Figure 6.

Involvement of the PGE_2 pathway in IDO1 expression by different cancer cell lines. **A,** Human tumor lines were treated with celecoxib. Quantification of *IDO1* was performed by RT-qPCR and reported to the untreated condition for each line (expressed in %). The transcript levels of *IDO1* per cell in the untreated conditions are described in Supplementary Table S1. **B,** MZ-CHA-3, LB919-SCCHN, LB188-SAR, and NCI-H596 were treated with AH6809 (EP2 inhibitor) while LB1610-MEL and SKOV3 were treated with GW627368X (EP4 inhibitor). Quantification of *IDO1* was performed by RT-qPCR. **C,** SKOV3 cells were treated with celecoxib at day 0. At day+2 cells were treated with the EP4 agonist for 24 hours before *IDO1* was quantified by RT-qPCR. **D,** U87 and A172 glioblastoma cells were treated 24 hours with an EP4 agonist. **E,** Tumor lines from the CCLE database were clustered into *IDO1*-positive and *IDO1*-negative lines and the expression of *COX-2* and *mPGES1* was compared. **F,** Table derived from the CCLE database illustrating the proportion of *IDO1*-expressing cell lines bearing mutations in the PI3K or MAPK pathways. **A–D**, Mean+SD of triplicates from one out of three experiments. (See also Supplementary Figs. S4 and S5.)

Published OnlineFirst July 21, 2017; DOI: 10.1158/2326-6066.CIR-16-0400

was required to jump-start constitutive *IDO1* expression. We therefore interrogated the CCLE database asking whether *IDO1*-expressing cell lines were enriched in PI3K or MAPK mutations. Indeed, we observed enrichment in MAPK or PI3K mutations in the *IDO1*-expressing cell lines. This was true in the whole set of cell lines and was confirmed in the subset of lung cancer, for which the number of cell lines was large enough (Fig. 6F).

No involvement of STAT3

One of the human tumor lines that we tested above, ovarian carcinoma SKOV3, was previously analyzed by Litzenburger and colleagues, who proposed that constitutive IDO1 expression was driven in this cell line by STAT3 activation, triggered by an autocrine loop of interleukin-6 (38). In fact, STAT3 has been described as a downstream effector of tyrosine kinase receptors, such as the EGF receptor or the IL6 receptor, but it can also be activated by the EP receptors (39). We therefore knocked down STAT3 in both SKOV3 and KUL98-MELA cells using a lentiviral shRNA construct. Although STAT3 was silenced in both cell lines, we observed no effect on IDO1 expression, neither at the mRNA level nor at the protein level (Supplementary Fig. S6A and S6C). Accordingly, IDO1 enzymatic activity was not reduced by STAT3 knockdown, although it was reduced in both cell lines by treatment with celecoxib (Supplementary Fig. S6B and S6D). Litzenburger and colleagues observed reduced IDO1 expression in SKOV3 cells after treatment with AG490, which was used as a JAK inhibitor. However, AG490 also inhibits EGFR (40) and thereby may inhibit the MAPK pathway and repress COX-2 expression. We observed that ruxolitinib, a more specific JAK1/2 inhibitor, abrogated the active phosphorylated form of STAT3 but did not reduce *IDO1* transcripts in both KUL98-MELA and SKOV3 cells (Supplementary Figs. S1A, S1B, and S6E). Altogether, these results do not support a direct role for STAT3 in IDO1 expression in SKOV3 and KUL98-MELA, but rather support the notion that constitutive IDO1 expression is driven by autocrine PGE_2. We do not exclude the possibility that STAT3 can induce IDO1 expression in specific contexts, but we propose that this effect might be indirect through the induction of COX-2 by STAT3 (41).

COX-2 inhibition promotes rejection of IDO1-expressing tumors

We set out to assess the relevance of our findings for cancer therapy. Because we could not identify a murine tumor line that expresses IDO1 constitutively, we set up an *in vivo* model using the human ovarian carcinoma line SKOV3 characterized above, which expresses IDO1 in a constitutive manner that is sensitive to celecoxib (Supplementary Fig. S7A and S7B). We injected SKOV3 cells into immunodeficient NOD/Scid/Il-2rg$^{-/-}$(NSG) mice (42). After 10 days, tumors were visible and mice received an injection of allogeneic human lymphocytes (PBMCs). Mice were also treated with celecoxib, and tumor growth was monitored (Fig. 7A). In the absence of celecoxib, tumor growth continued unabated at a rate similar to tumors of mice that did not receive human lymphocytes, indicating that the antitumor effect of allogeneic lymphocytes was blocked, possibly because of IDO1 expression by SKOV3 cells (Fig. 7B). In contrast, tumor growth was controlled in mice that received lymphocytes and celecoxib. Because the COX-2/PGE_2 axis may also favor tumor development by non-immune pathways such as angiogenesis, we also administered celecoxib to SKOV3 tumor–bearing mice that did not receive human lymphocytes. In this setting, celecoxib did not alter the course of tumor growth (Fig. 7B). In line with the notion that the tumor rejection promoted by celecoxib resulted from a blockade of IDO1 expression, we observed an identical antitumor effect in mice treated with allogeneic lymphocytes and IDO1 inhibitor epacadostat, which we confirmed can effectively block IDO1 enzymatic activity and restore proliferation of T lymphocytes cocultured with SKOV3 cells (Supplementary Fig. S7C and S7D). Conversely, when we repeated this experiment with IDO1-negative tumor colorectal carcinoma line LS411N, we observed some immune control with allogeneic lymphocytes in untreated mice, in line with the absence of IDO1 expression, but there was no additional effect of celecoxib or epacadostat (Fig. 7B, right). These results suggested that celecoxib treatment of mice bearing SKOV3 tumors repressed IDO1 expression in these tumors and thereby allowed lymphocyte infiltration and proliferation in the tumor. To confirm this interpretation, we first excluded a direct effect of celecoxib on human lymphocytes by measuring their proliferation and cytokine production *in vitro* in the presence or absence of celecoxib. No difference was observed in terms of proliferation and Th1 cytokine production, although Th2 cytokine production was reduced in the presence of celecoxib (Supplementary Fig. S7E and S7F). In contrast, proliferation and Th1 cytokine production were impaired when lymphocytes were cultured in SKOV3-conditioned medium, but not when they were cultured in medium conditioned with celecoxib-treated SKOV3 cells (Supplementary Fig. S7E and S7F). This is in line with the effect of celecoxib on IDO1 expression and tryptophan catabolism in SKOV3 cells (Supplementary Fig. S7A and S7B). Second, we tested IDO1 expression by Western blot in SKOV3 tumors collected from mice at day 7 of the *in vivo* experiment (Fig. 7C). In mice treated with celecoxib, IDO1 expression was reduced, particularly in mice that did not receive lymphocytes. Mice that did receive lymphocytes expressed residual amounts of IDO1 despite celecoxib. This residual expression, which probably resulted from IDO1 induction by IFNγ produced by lymphocytes, did not affect lymphocyte activity in this model, because we observed equal tumor control in mice that received lymphocytes with celecoxib, IDO1 inhibitor or both (Fig. 7B). Lastly, we analyzed T-cell infiltration in SKOV3 tumors collected at day 40 of the *in vivo* experiment. We stained tumor sections for CD3 and CD8 and observed a higher infiltration of both CD3-positive cells and CD8-positive cells in tumors from mice treated with celecoxib or epacadostat as compared to untreated mice (Fig. 7D and E). This was confirmed by RT-qPCR analysis of additional tumors (Fig. 7F). Altogether, these results confirmed the mechanism whereby celecoxib induced the rejection of SKOV3 tumors in this model. Celecoxib repressed IDO1 expression in SKOV3 tumor cells, thereby releasing the T-cell suppression imposed by tryptophan catabolism in the tumor microenvironment, and unleashing T cells that can now survive and proliferate at the tumor site to achieve tumor rejection.

Discussion

Certain human tumors of various histotypes express IDO1 in a constitutive manner, thereby setting up a mechanism of innate or intrinsic immune resistance that can prevent T-cell infiltration resulting in uninflamed or "cold" tumors. Such a mechanism differs from the adaptive immune resistance, initially described in

Published OnlineFirst July 21, 2017; DOI: 10.1158/2326-6066.CIR-16-0400

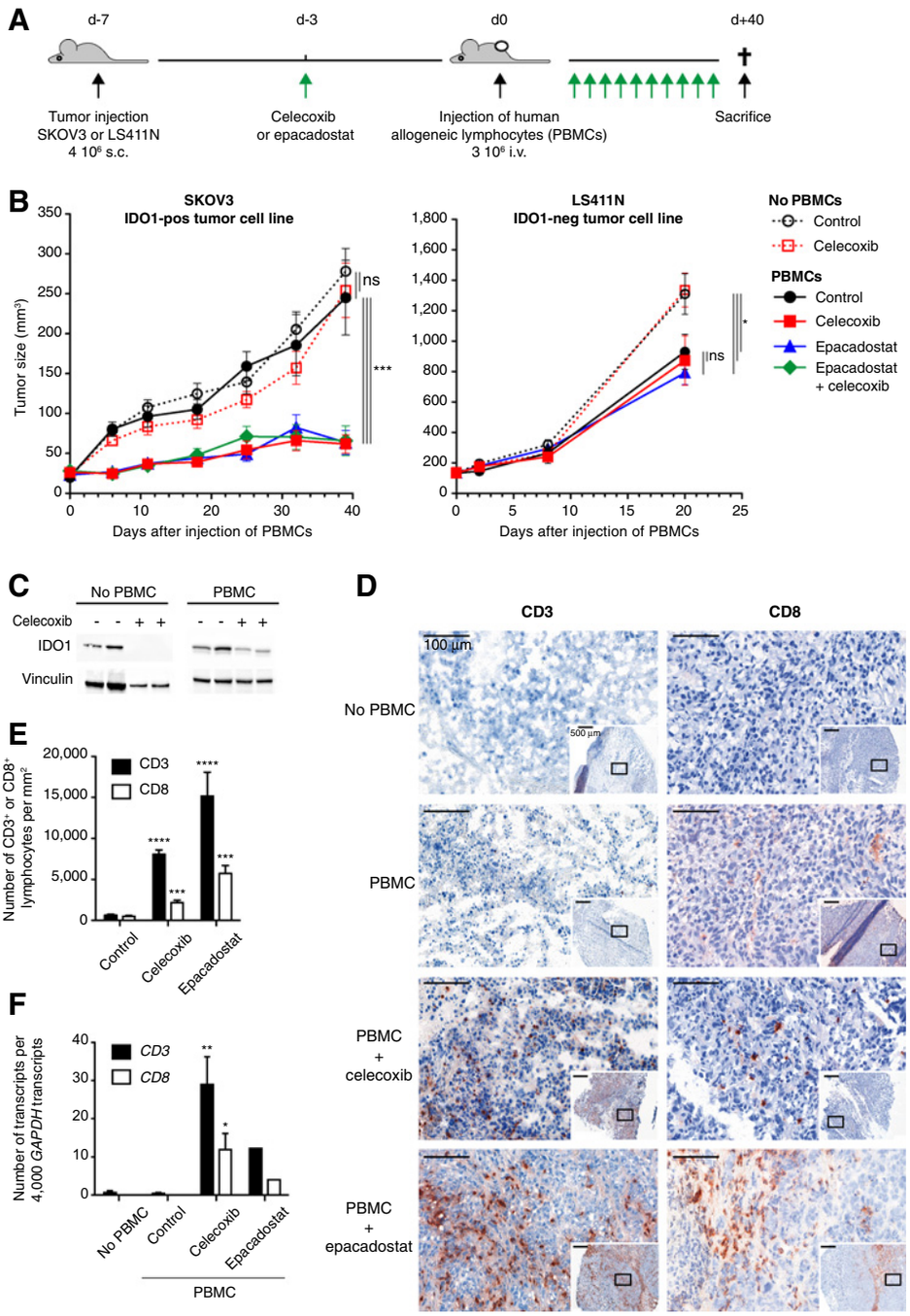

Figure 7.
Celecoxib favors immune rejection of IDO1-expressing human ovarian carcinoma. **A,** Scheme of the experimental procedure detailed in the Materials and Methods section. **B,** Tumor growth was measured twice a week until mice were sacrificed according to ethical recommendations. Mean ± SEM of 9 mice/group; experiment repeated 3–5 times for SKOV-3, once for LS411N. **C,** Tumors collected at d+7 were frozen, proteins were extracted and IDO1 expression was tested by Western blot (repeated 3 times). **D,** Illustration of the CD3 and CD8 immunohistochemistry stainings of frozen sections from one representative SKOV3 tumor for each of the indicated experimental conditions. 60× magnification (10× for the inset). **E,** Quantification by ImageJ software (whole sections) of the CD3 and CD8 stainings illustrated on panel **D** (Mean+SD). Statistics represent the comparison between the treated and the untreated conditions for each specific staining. **F,** Quantitative analysis of *CD3* and *CD8* transcripts in RNA from 4 tumors for each condition, collected in two separate experiments (1 tumor for the epacadostat condition) (Mean+SD). Statistics represent the comparison between the treated and the untreated conditions for each specific gene expression. See also Supplementary Fig. S7.

human melanoma, in which IDO1 expression is associated with T-cell infiltration and triggered by the interferon-gamma produced by infiltrating T cells. Because immune checkpoint inhibitors act by unleashing existing antitumor T lymphocytes, they are more efficient in patients bearing T-cell inflamed tumors than in those with uninflamed or cold tumors. Defining new approaches to trigger T-cell infiltration in cold tumors will be key to increasing the efficacy of cancer immunotherapy. This requires a detailed understanding of the molecular mechanisms responsible for this lack of T-cell infiltration.

Here, we characterized the signaling mechanisms responsible for constitutive IDO1 expression in a series of human tumors of various types. We found that constitutive IDO1 expression was dependent on an autocrine loop of PGE_2 production, leading to activation of the PI3K and PKC pathways and the subsequent activation of *IDO1* transcription by factors such as β-catenin and, most likely, ETV4. Autocrine PGE_2 production depends on constitutive expression of mPGES1 and COX-2. The latter is controlled by the MAPK pathway, which can be activated in tumor cells by growth factors such as IL1 or EGF, but can also be activated

Published OnlineFirst July 21, 2017; DOI: 10.1158/2326-6066.CIR-16-0400

by oncogenic mutations such as *BRAF* V600E. Indeed, inhibition of mutant *BRAF* in melanoma line KUL98-MELA suppressed both COX-2 and IDO1 expression. Our results therefore provide a conceptual framework to explain the role of COX-2 as a driver of tumor-induced immunosuppression (20, 21). In Zelenay and colleagues, inhibition or ablation of COX-2 in a *BRAF* V600E mouse melanoma model rendered tumors sensitive to immune control (20). In Hou and colleagues, PGE_2 inactivation sensitized tumors to immunotherapy (21). Our results suggest that at least part of the effect reported in these studies may have been mediated by the repression of IDO1 expression in those tumors.

We observed that most of the tumor lines that express IDO1 constitutively also bear oncogenic mutations in one of the signaling pathways involved in the autocrine loop we describe, including PI3K and MAPK. An analysis of the CCLE database confirmed that IDO1-expressing tumor lines harbored mutations in the PI3K or MAPK pathways more frequently than IDO1-negative lines, suggesting that oncogenic signaling jump-starts IDO1 expression.

A similar case has been described for PD-L1, another immunosuppressive factor whose expression can either be induced by interferon-gamma produced by infiltrating T cells, resulting in adaptive immune resistance, or be constitutive, leading to intrinsic (or innate) immune resistance (19). The mechanisms responsible for constitutive PD-L1 expression in human tumors have only begun to be characterized, and appear to involve the PI3K/AKT axis in glioblastomas (43) and triple-negative breast carcinomas (44), whereas Hodgkin lymphomas express PD-L1 as a result of the amplification of the encoding gene (45).

Our results suggest potential therapeutic avenues that may be useful to treat cold tumors. Besides inhibitors of IDO1 enzymatic activity, which are in phase III of clinical evaluation, COX-2 inhibitors can prevent IDO1 expression in those tumors. We validated this prediction using human SKOV3 tumors in NSG mice reconstituted with human allogeneic lymphocytes. These tumors were not rejected unless mice were treated with a COX-2 inhibitor or with an IDO1 inhibitor. Although PGE_2 may trigger other immunosuppressive mechanisms in different contexts (46), the lack of additive antitumor effect of targeting both COX-2 and IDO1 supports the notion that the effect of celecoxib in our model is essentially mediated by repression of IDO1 expression. Although we did not test the effect of PI3K, mTOR, MAPK, or *BRAF* V600E inhibitors in this *in vivo* model, it is possible that IDO1 repression contributes to the antitumor effects observed with such molecules in other contexts. PI3K contributes to the induction of long-term immune tolerance by mouse plasmacytoid dendritic cells (pDC) that have been exposed to TGFβ. PI3K promotes phosphorylation of IDO1 by the Fyn tyrosine kinase, thereby inducing a signaling pathway that results in sustained expression of IDO1 and TGFβ (47). PI3K inhibition would therefore not only reduce IDO1 constitutive expression in cancer cells but also abrogate tolerance induction by pDCs in the tumor microenvironment. This double effect would favor tumor rejection. In sum, our results further highlight the potential of COX-2 and, potentially, PI3K inhibitors as useful adjuvants to combine with cancer immunotherapy.

Imatinib, which is used in the treatment of gastrointestinal stromal tumors (GIST) for its ability to inhibit oncogenic signaling due to mutant *KIT* or *PDGFR*, also represses IDO1 expression in those tumors and thereby favors their control by antitumor T lymphocytes (32). In line with our findings in other tumor types, oncogenic *KIT* signaling in GIST involves the PI3K–AKT–mTOR pathway and culminates in the induction of ETV4, a transcription factor whose expression is repressed in imatinib-treated GIST cells. ETV4 binding sites were identified in the *IDO1* promoter and confirmed to bind ETV4 by chromatin immunoprecipitation (32). Hence, ETV4 may link the PI3K–AKT–mTOR pathway to the activation of the *IDO1* promoter (Fig. 2). However, other transcription factors downstream of mTOR may also play a role.

Our results also indicate that β-catenin likely links the PKC-GSK3β pathway to the activation of the *IDO1* promoter (Fig. 2). In melanoma, intrinsic β-catenin signaling is a key factor mediating immune resistance and lack of T-cell infiltration (33, 48). This study identified ATF3-mediated repression of chemokine CCL4 as responsible for the lack of recruitment of $CD103^+$ dendritic cells in the tumor and the resulting lack of T-cell infiltration. Based on our results, we speculate that β-catenin signaling also prevents T-cell infiltration by inducing constitutive expression of IDO1.

By deciphering the oncogenic signaling pathways responsible for constitutive IDO1 expression in human tumors, our results shed light on the mechanisms responsible for the problem of cold tumors, which are not infiltrated by T lymphocytes and therefore fail to respond to immunotherapy. Our results also suggest clinically applicable therapeutic options to counteract such immunosuppressive mechanisms.

Disclosure of Potential Conflicts of Interest

B.J. Van den Eynde is a member of the board of directors for, has ownership in, and is a consultant/advisory board member of Iteos Therapeutics. No potential conflicts of interest were disclosed by the other authors.

Authors' Contributions

Conception and design: M. Hennequart, L. Pilotte, E. De Plaen, B.J. Van den Eynde

Development of methodology: M. Hennequart, L. Pilotte, S. Cane, E. De Plaen, B.J. Van den Eynde

Acquisition of data (provided animals, acquired and managed patients, provided facilities, etc.): M. Hennequart, L. Pilotte, D. Hoffmann, V. Stroobant, E. De Plaen

Analysis and interpretation of data (e.g., statistical analysis, biostatistics, computational analysis): M. Hennequart, L. Pilotte, V. Stroobant, E. De Plaen, B.J. Van den Eynde

Writing, review, and/or revision of the manuscript: M. Hennequart, L. Pilotte, E. De Plaen, B.J. Van den Eynde

Administrative, technical, or material support (i.e., reporting or organizing data, constructing databases): M. Hennequart, L. Pilotte, E. De Plaen, B.J. Van den Eynde

Study supervision: B.J. Van den Eynde

Acknowledgments

We thank Guy Warnier, Gilles Gaudray, Julien Gossiaux, and Laurent Hermans for production of NOD/Scid/Il-2rg$^{-/-}$ (NSG) mice; Sophie Lucas, Catherine Uyttenhove, and Stéphanie Liénart for advice on the NSG experiment; Céline Bugli for statistical advice; Pierre van der Bruggen and Pierre Coulie for critical comments; and Auriane Sibille for editorial assistance.

Grant Support

This work was supported by Ludwig Cancer Research, Walloon Excellence in Life Sciences and Biotechnology (WELBIO, Belgium), FNRS-Télévie (Belgium), Foundation Against Cancer (Belgium), de Duve Institute and Université catholique de Louvain (Belgium). M. Hennequart was supported by FNRS-Télévie (Grant number: 7.4590.15), L. Pilotte by de Duve Institute, S. Cane by

FNRS-Télévie (Grant number: 7.4538.14), D. Hoffmann by FRIA (Grant number: 1.E082.14), and V. Stroobant, E. De Plaen, and B.J. Van den Eynde by the Ludwig Institute for Cancer Research.

The costs of publication of this article were defrayed in part by the payment of page charges. This article must therefore be hereby marked *advertisement* in accordance with 18 U.S.C. Section 1734 solely to indicate this fact.

Received December 29, 2016; revised May 2, 2017; accepted June 30, 2017; published OnlineFirst July 21, 2017.

References

1. Sharma P, Allison JP. The future of immune checkpoint therapy. Science 2015;348:56–61.
2. McGaha TL, Huang L, Lemos H, Metz R, Mautino M, Prendergast GC, et al. Amino acid catabolism: a pivotal regulator of innate and adaptive immunity. Immunol Rev 2012;249:135–57.
3. van Baren N, Van den Eynde BJ. Tumoral immune resistance mediated by enzymes that degrade tryptophan. Cancer Immunol Res 2015;3:978–85.
4. Munn DH, Sharma MD, Baban B, Harding HP, Zhang Y, Ron D, et al. GCN2 kinase in T cells mediates proliferative arrest and anergy induction in response to indoleamine 2,3-dioxygenase. Immunity 2005;22:633–42.
5. Terness P, Bauer TM, Röse L, Dufter C, Watzlik A, Simon H, et al. Inhibition of allogeneic T cell proliferation by indoleamine 2,3-dioxygenase-expressing dendritic cells: mediation of suppression by tryptophan metabolites. J Exp Med 2002;196:447–57.
6. Cobbold SP, Adams E, Farquhar CA, Nolan KF, Howie D, Lui KO, et al. Infectious tolerance via the consumption of essential amino acids and mTOR signaling. Proc Natl Acad Sci USA 2009;106:12055–60.
7. Munn DH, Zhou M, Attwood JT, Bondarev I, Conway SJ, Marshall B, et al. Prevention of allogeneic fetal rejection by tryptophan catabolism. Science 1998;281:1191–3.
8. Mellor AL, Munn DH. IDO expression by dendritic cells: tolerance and tryptophan catabolism. Nat Rev Immunol 2004;4:762–74.
9. Theate I, van Baren N, Pilotte L, Moulin P, Larrieu P, Renauld JC, et al. Extensive profiling of the expression of the indoleamine 2,3-dioxygenase 1 protein in normal and tumoral human tissues. Cancer Immunol Res 2015;3:161–72.
10. Konan KV, Taylor MW. Importance of the two interferon-stimulated response element (ISRE) sequences in the regulation of the human indoleamine 2,3-dioxygenase gene. J Biol Chem 1996;271:19140–5.
11. Chon SY, Hassanain HH, Gupta SL. Cooperative role of interferon regulatory factor 1 and p91 (STAT1) response elements in interferon-gamma-inducible expression of human indoleamine 2,3-dioxygenase gene. J Biol Chem 1996;271:17247–52.
12. Chang MY, Smith C, DuHadaway JB, Pyle JR, Boulden J, Soler AP, et al. Cardiac and gastrointestinal liabilities caused by deficiency in the immune modulatory enzyme indoleamine 2,3-dioxygenase. Cancer Biol Ther 2011;12:1050–8.
13. Uyttenhove C, Pilotte L, Theate I, Stroobant V, Colau D, Parmentier N, et al. Evidence for a tumoral immune resistance mechanism based on tryptophan degradation by indoleamine 2,3-dioxygenase. Nat Med 2003;9:1269–74.
14. Koblish HK, Hansbury MJ, Bowman KJ, Yang G, Neilan CL, Haley PJ, et al. Hydroxyamidine inhibitors of indoleamine-2,3-dioxygenase potently suppress systemic tryptophan catabolism and the growth of IDO-expressing tumors. Mol Cancer Ther 2010;9:489–98.
15. Brandacher G, Perathoner A, Ladurner R, Schneeberger S, Obrist P, Winkler C, et al. Prognostic value of indoleamine 2,3-dioxygenase expression in colorectal cancer: effect on tumor-infiltrating T cells. Clin Cancer Res 2006;12:1144–51.
16. Ino K, Yamamoto E, Shibata K, Kajiyama H, Yoshida N, Terauchi M, et al. Inverse correlation between tumoral indoleamine 2,3-dioxygenase expression and tumor-infiltrating lymphocytes in endometrial cancer: its association with disease progression and survival. Clin Cancer Res 2008;14:2310–7.
17. Inaba T, Ino K, Kajiyama H, Yamamoto E, Shibata K, Nawa A, et al. Role of the immunosuppressive enzyme indoleamine 2,3-dioxygenase in the progression of ovarian carcinoma. Gynecol Oncol 2009;115:185–92.
18. Spranger S, Koblish HK, Horton B, Scherle PA, Newton R, Gajewski TF. Mechanism of tumor rejection with doublets of CTLA-4, PD-1/PD-L1, or IDO blockade involves restored IL-2 production and proliferation of CD8(+) T cells directly within the tumor microenvironment. J Immunother Cancer 2014;2:3.
19. Topalian SL, Drake CG, Pardoll DM. Immune checkpoint blockade: a common denominator approach to cancer therapy. Cancer Cell 2015;27:450–61.
20. Zelenay S, van der Veen AG, Bottcher JP, Snelgrove KJ, Rogers N, Acton SE, et al. Cyclooxygenase-dependent tumor growth through evasion of immunity. Cell 2015;162:1257–70.
21. Hou W, Sampath P, Rojas JJ, Thorne SH. Oncolytic virus-mediated targeting of PGE2 in the tumor alters the immune status and sensitizes established and resistant tumors to immunotherapy. Cancer Cell 2016;30:108–19.
22. Gobel C, Breitenbuecher F, Kalkavan H, Hahnel PS, Kasper S, Hoffarth S, et al. Functional expression cloning identifies COX-2 as a suppressor of antigen-specific cancer immunity. Cell Death Dis 2014;5:e1568.
23. Pilotte L, Larrieu P, Stroobant V, Colau D, Dolusic E, Frederick R, et al. Reversal of tumoral immune resistance by inhibition of tryptophan 2,3-dioxygenase. Proc Natl Acad Sci USA 2012;109:2497–502.
24. Davis LG, Dibner MD, Battey JF. Guanidine isothiocyanate preparation of total RNA. In:Davis LG, Dibner MD, Battey JF, editors. Basic Methods in Molecular Biology. New York: Elsevier; 1986. p130–5.
25. von Bergwelt-Baildon MS, Popov A, Saric T, Chemnitz J, Classen S, Stoffel MS, et al. CD25 and indoleamine 2,3-dioxygenase are up-regulated by prostaglandin E2 and expressed by tumor-associated dendritic cells in vivo: additional mechanisms of T-cell inhibition. Blood 2006;108:228–37.
26. Fujino H, West KA, Regan JW. Phosphorylation of glycogen synthase kinase-3 and stimulation of T-cell factor signaling following activation of EP2 and EP4 prostanoid receptors by prostaglandin E2. J Biol Chem 2002;277:2614–9.
27. Regan JW. EP2 and EP4 prostanoid receptor signaling. Life Sci 2003;74:143–53.
28. Castellone MD, Teramoto H, Williams BO, Druey KM, Gutkind JS. Prostaglandin E2 promotes colon cancer cell growth through a Gs-axin-beta-catenin signaling axis. Science 2005;310:1504–10.
29. Sarker D, Ang JE, Baird R, Kristeleit R, Shah K, Moreno V, et al. First-in-human phase I study of pictilisib (GDC-0941), a potent pan-class I phosphatidylinositol-3-kinase (PI3K) inhibitor, in patients with advanced solid tumors. Clin Cancer Res 2015;21:77–86.
30. Fang X, Yu S, Tanyi JL, Lu Y, Woodgett JR, Mills GB. Convergence of multiple signaling cascades at glycogen synthase kinase 3: Edg receptor-mediated phosphorylation and inactivation by lysophosphatidic acid through a protein kinase C-dependent intracellular pathway. Mol Cell Biol 2002;22:2099–110.
31. Soichot M, Hennart B, Al Saabi A, Leloire A, Froguel P, Levy-Marchal C, et al. Identification of a variable number of tandem repeats polymorphism and characterization of LEF-1 response elements in the promoter of the IDO1 gene. PLoS One 2011;6:e25470.
32. Balachandran VP, Cavnar MJ, Zeng S, Bamboat ZM, Ocuin LM, Obaid H, et al. Imatinib potentiates antitumor T cell responses in gastrointestinal stromal tumor through the inhibition of Ido. Nat Med 2011;17:1094–100.
33. Spranger S, Bao R, Gajewski TF. Melanoma-intrinsic beta-catenin signalling prevents anti-tumour immunity. Nature 2015;523:231–5.
34. Tsatsanis C, Androulidaki A, Venihaki M, Margioris AN. Signalling networks regulating cyclooxygenase-2. Int J Biochem Cell Biol 2006;38:1654–61.
35. Park EJ, Kwon TK. Rottlerin enhances IL-1beta-induced COX-2 expression through sustained p38 MAPK activation in MDA-MB-231 human breast cancer cells. Exp Mol Med 2011;43:669–75.
36. Walters JN, Bickford JS, Newsom KJ, Beachy DE, Barilovits SJ, Herlihy JD, et al. Regulation of human microsomal prostaglandin E synthase-1 by IL-1beta requires a distal enhancer element with a unique role for C/EBPbeta. Biochem J 2012;443:561–71.
37. El Mansouri FE, Nebbaki SS, Kapoor M, Afif H, Martel-Pelletier J, Pelletier JP, et al. Lysine-specific demethylase 1-mediated demethylation of histone H3 lysine 9 contributes to interleukin 1beta-induced microsomal

prostaglandin E synthase 1 expression in human osteoarthritic chondrocytes. Arthritis Res Ther 2014;16:R113.
38. Litzenburger UM, Opitz CA, Sahm F, Rauschenbach KJ, Trump S, Winter M, et al. Constitutive IDO expression in human cancer is sustained by an autocrine signaling loop involving IL-6, STAT3 and the AHR. Oncotarget 2014;5:1038–51.
39. Han C, Demetris AJ, Stolz DB, Xu L, Lim K, Wu T. Modulation of Stat3 activation by the cytosolic phospholipase A2alpha and cyclooxygenase-2-controlled prostaglandin E2 signaling pathway. J Biol Chem 2006;281: 24831–46.
40. Caceres-Cortes JR. A potent anti-carcinoma and anti-acute myeloblastic leukemia agent, AG490. Anticancer Agents Med Chem 2008;8:717–22.
41. Xiong H, Du W, Sun TT, Lin YW, Wang JL, Hong J, et al. A positive feedback loop between STAT3 and cyclooxygenase-2 gene may contribute to Helicobacter pylori-associated human gastric tumorigenesis. Int J Cancer 2014;134:2030–40.
42. Shultz LD, Brehm MA, Garcia-Martinez JV, Greiner DL. Humanized mice for immune system investigation: progress, promise and challenges. Nat Rev Immunol 2012;12:786–98.
43. Parsa AT, Waldron JS, Panner A, Crane CA, Parney IF, Barry JJ, et al. Loss of tumor suppressor PTEN function increases B7-H1 expression and immunoresistance in glioma. Nat Med 2007;13:84–8.
44. Mittendorf EA, Philips AV, Meric-Bernstam F, Qiao N, Wu Y, Harrington S, et al. PD-L1 expression in triple-negative breast cancer. Cancer Immunol Res 2014;2:361–70.
45. Green MR, Monti S, Rodig SJ, Juszczynski P, Currie T, O'Donnell E, et al. Integrative analysis reveals selective 9p24.1 amplification, increased PD-1 ligand expression, and further induction via JAK2 in nodular sclerosing Hodgkin lymphoma and primary mediastinal large B-cell lymphoma. Blood 2010;116:3268–77.
46. Liu B, Qu L, Yan S. Cyclooxygenase-2 promotes tumor growth and suppresses tumor immunity. Cancer Cell Int 2015;15:106.
47. Pallotta MT, Orabona C, Volpi C, Vacca C, Belladonna ML, Bianchi R, et al. Indoleamine 2,3-dioxygenase is a signaling protein in long-term tolerance by dendritic cells. Nat Immunol 2011;12:870–8.
48. Spranger S, Gajewski TF. A new paradigm for tumor immune escape: beta-catenin-driven immune exclusion. J Immunother Cancer 2015; 3:43.

Published OnlineFirst July 21, 2017; DOI: 10.1158/2326-6066.CIR-16-0400

Cancer Immunology Research

Constitutive IDO1 Expression in Human Tumors Is Driven by Cyclooxygenase-2 and Mediates Intrinsic Immune Resistance

Marc Hennequart, Luc Pilotte, Stefania Cane, et al.

Cancer Immunol Res 2017;5:695-709. Published OnlineFirst July 21, 2017.